DFTT 49/97

Pinning down neutralino properties from a possible modulation signal in WIMP direct search

A. Bottino[a] *, F. Donato[a], N. Fornengo[a], S. Scopel[b†]

[a] *Dipartimento di Fisica Teorica, Università di Torino and INFN, Sezione di Torino, Via P. Giuria 1, 10125 Torino, Italy*
[b] *Instituto de Física Nuclear y Altas Energías, Facultad del Ciencias, Universidad de Zaragoza, Plaza de San Francisco s/n, 50009 Zaragoza, Spain*

(September 7, 1997)

Abstract

We analyze the properties of neutralino under the hypothesis that some preliminary experimental results of the DAMA/NaI Collaboration may be indicative of a yearly modulation effect. We examine which supersymmetric configurations would be singled out by the DAMA/NaI data. We also discuss the possibility to investigate these configurations by means of experimental searches for relic neutralinos other than direct searches. We finally discuss the possibility to probe these configurations by accelerator searches.

Typeset using REVTEX

*E–mail: bottino@to.infn.it,donato@to.infn.it, fornengo@to.infn.it,scopel@ezar76.unizar.es

†INFN Post–doctoral Fellow

I. INTRODUCTION

In Ref. [1] it was shown that the DAMA/NaI experiment for direct WIMP search, which uses a large-mass, low-background NaI (Tl) detector at the Gran Sasso Laboratory [2], has currently a sensitivity good enough to investigate relic neutralinos in sizeable regions of the supersymmetric parameter space. It was also noticed in Ref. [1] that this is the prerequisite for a significant study of a yearly modulation effect, which appears to be the main experimental mean available at present for an efficient signal/background discrimination in direct relic-particle detection. Other interesting experimental strategies for disentangling a WIMP signal from the background are still at an R&D stage [3].

It is now reported by the DAMA/NaI Collaboration an analysis of a collection of data over an exposure of 4549 Kg $\times$ days: 3363.8 Kg $\times$ days during the winter, 1185.2 Kg $\times$ days during the summer, obtained with an experimental set-up consisting of nine 9.70 Kg NaI(Tl) detectors [4]. A stability control of the apparatus, based on the ^{210}Pb peak at 46.5 KeV, allowed the DAMA/NaI Collaboration to analyse their data in terms of a yearly modulation effect. The technique for the extraction of a possible signal is a maximum likelihood method applied to a binning in the recoil energy of the daily counts per detector. The most intriguing result of the investigation carried out in Ref. [4] is that their set of data appears to be compatible with no-modulation only at a 10% probability level. When interpreted in terms of a modulation signal due to a WIMP of mass m_χ and scalar elastic cross section (off nucleon) $\sigma_{\rm scalar}^{\rm (nucleon)}$, the data of Ref. [4] single out (at 90% C.L.) the region of Fig.1, which is delimited by a closed contour (hereafter defined as region R_m). The open curve in Fig.1 denotes the 90% C.L. upper bound of $\sigma_{\rm scalar}^{\rm (nucleon)}$, as obtained from the total counting rates of Ref. [2]. Both open and closed contour lines were obtained employing for the astrophysical parameters the set I of Table 1 (notice that the relevant lines of Fig.1 of Ref. [4] correspond to the value $\rho_l = 0.3$ GeV cm^{-3} for the local dark matter density, instead of the value $\rho_l = 0.5$ GeV cm^{-3} adopted here).

As stressed in Ref. [4], the occurrence of region R_m as a domain relevant for a possible modulation effect will require further investigation with experimental runs with a much higher statistics. Meanwhile, in view of the relevance of the issue at stake, we consider of great interest to analyse the following questions: a) what would be the features of a neutralino (as a definite WIMP candidate) to satisfy the prerequisites of region R_m; b) would any other experimental search for relic neutralinos be able to investigate the region R_m; c) are neutralino configurations of region R_m accessible to accelerator searches in the near future? The present paper addresses all of these questions. Point a) will be analysed in the Minimal Supersymmetric extension of the Standard Model (MSSM) [5]. As far as point b) is concerned, we consider here the possible signals of up–going muons which would be originated by neutralino–neutralino annihilation inside the Earth or the Sun [6–8], and, as for point c), we will mainly concentrate on the discovery potential at LEP and Tevatron.

The plan of this letter is the following. In Section II we present the theoretical scheme adopted for our analysis and for our calculation of the relevant quantities for direct and indirect detection of relic neutralinos. Section III is devoted to the discussion of the properties of the neutralino configurations of region R_m which survive the current bounds from indirect detection. In Section IV we conclude with some final comments.

II. SUPERSYMMETRIC MODEL

The WIMP candidate considered in this paper is the neutralino, defined as the lowest–mass linear superposition of photino ($\tilde{\gamma}$), zino ($\tilde{Z}$) and the two higgsino states ($\tilde{H}_1^\circ$, $\tilde{H}_2^\circ$)

$$\chi \equiv a_1\tilde{\gamma} + a_2\tilde{Z} + a_3\tilde{H}_1^\circ + a_4\tilde{H}_2^\circ, \tag{1}$$

In this paper we employ the Minimal Supersymmetric extension of the Standard Model MSSM) [5]. This model is convenient to describe the supersymmetric phenomenology at the electroweak scale without too strong theoretical assumptions. Various properties (relic abundances and detection rates) of relic neutralinos have been analyzed in the MSSM by a number of authors. Some of the most recent papers are given in Refs. [1,6–13].

The MSSM is based on the same gauge group as the Standard Model and contains the supersymmetric extension of its particle content. In order to give mass both to down– and up–type quarks and to cancel anomalies, two Higgs doublets H_1 and H_2 are necessary. As a consequence, the MSSM contains three neutral Higgs fields: two of them are scalar fields, the other is a pseudoscalar particle. At the tree level the Higgs sector is specified by two independent parameters: the mass of one of the physical Higgs fields, which we choose to be the mass m_A of the neutral pseudoscalar boson, and the ratio of the two vacuum expectation values, defined as $\tan\beta \equiv \langle H_2\rangle/\langle H_1\rangle$. Once radiative corrections are introduced, the Higgs sector depends also on the squark masses through loop diagrams. The other parameters of the model are defined in the superpotential, which contains all the Yukawa interactions and the Higgs–mixing term $\mu H_1 H_2$, and in the soft–breaking Lagrangian, which contains the trilinear and bilinear breaking parameters and the soft gaugino and scalar mass terms.

As it stands, the MSSM contains a large number of free parameters. Therefore, in order to deal with manageable models, it is necessary to introduce some assumptions which establish relations among the parameters at the electroweak scale. The usual conditions, which are also employed here, are the following: i) all trilinear parameters are set to zero except those of the third family, which are unified to a common value A; ii) all squarks and sleptons soft–mass parameters are taken as degenerate: $m_{\tilde{l}_i} = m_{\tilde{q}_i} \equiv m_0$, iii) the gaugino masses are assumed to unify at M_{GUT}, and this implies that the $U(1)$ and $SU(2)$ gaugino masses are related at the electroweak scale by $M_1 = (5/3)\tan^2\theta_W M_2$.

After these conditions are applied, the supersymmetric parameter space consists of six independent parameters. We choose them to be: $M_2, \mu, \tan\beta, m_A, m_0, A$. We vary these parameters in the following ranges: 10 GeV $\leq M_2 \leq$ 500 GeV, 10 GeV $\leq |\mu| \leq$ 500 GeV, 65 GeV $\leq m_A \leq$ 500 GeV, 100 GeV $\leq m_0 \leq$ 500 GeV, $-3 \leq$ A $\leq +3$, $1.01 \leq \tan\beta \leq 50$.

In our analysis the supersymmetric parameter space is constrained by all the experimental limits obtained from accelerators on supersymmetric and Higgs searches. In particular, the latest data from LEP2 on Higgs, neutralino, chargino and sfermion masses are used [14]. Moreover, the constraints due to the $b \to s + \gamma$ process [15] are satisfied. In addition to the experimental limits, we further constrain the parameter space by requiring that the neutralino is the Lightest Supersymmetric Particle (LSP), i.e., regions where the gluino or squarks or sleptons are lighter than the neutralino are excluded. This requirement is necessary for the neutralino to be the WIMP candidate. Finally, the regions of the parameter

space where the neutralino relic abundance exceeds the cosmological bound, i.e. $\Omega_\chi h^2 > 1$, are also excluded.

A. Scalar χ–nucleus cross section

Neutralinos interact with matter both through coherent effects [16,17] and spin–dependent interactions [17]. In the present paper we confine ourselves to the coherent effects, since these are the only ones which, with the current experimental sensitivities, are actually most easily accessible to direct detection.

The pointlike χ–nucleus coherent cross–section is given by

$$\sigma_C^0 = \frac{8G_F^2}{\pi} M_Z^2 \zeta^2 m_{\rm red}^2 A_N^2 \,, \tag{2}$$

where G_F is the Fermi constant, M_Z is the Z boson mass and A_N and $m_{\rm red}$ are the nucleus mass number and the neutralino–nucleus reduced mass, respectively. The quantity ζ, which depends on the χ–quark couplings mediated by Higgs particles and squarks, were originally evaluated in Refs. [16,17]. The full expression for ζ together with the values used here for the relevant parameters are reported in Ref. [18].

Due to the structure of Eq.(2) an equivalent χ–nucleon scalar cross–section may be defined as

$$\sigma_{\rm scalar}^{\rm (nucleon)} = \left(\frac{1 + m_\chi/m_N}{1 + m_\chi/m_P} \right)^2 \frac{\sigma_C^0}{A_N^2} \tag{3}$$

where m_N (m_P) is the nuclear (proton) mass. The connection between Eq.(3) and the differential event rate for elastic neutralino–nucleus scattering may be found in Ref. [1].

B. Relic abundance and scaling factor ξ

The relevant quantity, dependent on the supersymmetric parameters, which enters in the event rate of direct detection as well as in the indirect signals considered in Sect.II C, is $\rho_\chi \times \sigma_{\rm scalar}^{\rm (nucleon)}$, where ρ_χ is the neutralino local (solar neighbourhood) density. We factorize ρ_χ as $\rho_\chi = \xi \rho_l$, i.e. in terms of the (total) local dark matter density ρ_l. Here ξ is calculated in the following way. For each point of the parameter space, we take into account the relevant value of the cosmological neutralino relic density. When $\Omega_\chi h^2$ is larger than a minimal value $(\Omega h^2)_{\rm min}$, compatible with observational data and with large–scale structure calculations, we simply put $\xi = 1$. When $\Omega_\chi h^2$ turns out to be less than $(\Omega h^2)_{\rm min}$, and then the neutralino may only provide a fractional contribution $\Omega_\chi h^2/(\Omega h^2)_{\rm min}$ to Ωh^2, we take $\xi = \Omega_\chi h^2/(\Omega h^2)_{\rm min}$. The value to be assigned to $(\Omega h^2)_{\rm min}$ is somewhat arbitrary, in the range $0.03 \lesssim (\Omega h^2)_{\rm min} \lesssim 0.3$. The values adopted in our calculations are listed in Table 1.

The neutralino relic abundance is evaluated here as discussed in Ref. [9]. Possible refinements due to the inclusion of coannihilation effects [10,19] do not appear to be essential here, since for the neutralino configurations discussed in this paper, the mass degeneracy of the LSP with the chargino and the next–to–lightest neutralino is always greater than 15–20%.

Only a few configurations, where the neutralino is mainly a higgsino, show a mass degeneracy LSP–chargino of the order of 10%. However, these configurations do not provide a cosmologically relevant neutralino, since $\Omega_\chi h^2 \lesssim 0.01$. The mass degeneracy with sfermions is also very marginal and does not modify the main results of our analysis.

C. Comparison with the experimental data of direct detection

We are now in the position to compare the data of Ref. [4] with our calculation within the MSSM scheme. The comparison is shown in Fig.1, where our results are provided in the form of a scatter plot, obtained by varying the parameters of the supersymmetric model in the intervals quoted above. To be definite, only positive values of μ are displayed in Fig.1, and all the discussion which follows refers to this case. We will comment on configurations belonging to $\mu < 0$ in Sect.III.

It is worth reminding that the density of the points in the scatter plot has no physical meaning, since it depends on the grid employed in the scanning of the supersymmetric parameter space. The main significant information from the theoretical scatter plot is provided by its contour. Also, we wish to point out that the large spread in the values of $\xi\sigma_{\rm scalar}^{\rm (nucleon)}$ reflects the ignorance in the physical values of the various supersymmetric parameters.

We see that our scatter plot of Fig.1 reaches abundantly the curve of the 90% C.L. bound and also populates the major part of the region R_m. These features show that: 1) the sensitivity of the DAMA/NaI experiment is adequate for a significant exploration of the neutralino parameter space; 2) many physical neutralino configurations are actually compatible with a modulation effect with values of m_χ and $\sigma_{\rm scalar}^{\rm (nucleon)}$ in the region R_m.

We will hereafter call S the set of neutralino configurations whose representative points fall inside R_m. In the following subsection we will apply to the set S the current experimental bounds due to neutralino–neutralino annihilation inside the Earth and the Sun.

D. χ–χ annihilation in the Earth and in the Sun

Signals of up–going muons generated by ν_μ's produced in pair annihilation of neutralinos in celestial macroscopic bodies have been analyzed by many authors. Some of the most recent papers in this field are given in Ref. [6–8,20].

The up–going muon fluxes Φ_μ reported here have been calculated with the procedure discussed in Refs. [7,20]. The values of these fluxes from the Earth, $\Phi_\mu^{\rm Earth}$, and from the Sun, $\Phi_\mu^{\rm Sun}$, for the configurations of set S are displayed in Figs.2a–b together with the experimental 90% C.L. upper bounds of Ref. [21] (similar bounds are also provided by MACRO [22].) In Fig.2a the prominent peak around $m_\chi \simeq 60$ GeV is due to the enhancement of the elastic χ–nucleus cross section, because of the mass matching of m_χ with the mass of the ^{56}Fe nucleus, which is a dominant element in the Earth composition.

From Figs.2a–b it turns out that many configurations of set S are disfavored by the present bounds on the up–going muon fluxes. However, it is remarkable that still a large portion of set S survives the indirect search bounds. Fig.3, when compared with Fig.1, shows how the limits due to $\Phi_\mu^{\rm Earth}$ and $\Phi_\mu^{\rm Sun}$ restrict the neutralino configurations singled

out by modulation effects in direct search (in Fig.3 all configurations falling out of region R_m have been dropped). We will denote by T the set of configurations, belonging to set S, which satisfy the bounds on the muon fluxes Φ_μ.

III. PROPERTIES OF THE NEUTRALINO ALLOWED STATES

Let us now consider the features of the supersymmetric configurations of set T. Some of these properties are displayed in Figs.4–7.

First, we discuss the parameters which determine the neutralino sector, namely M_2, μ and $\tan\beta$. In Fig.4 we display the physical region of neutralino configurations of set T. Dots denote configurations with $10 \leq \tan\beta < 50$, stars denote configurations with $5 \leq \tan\beta < 50$ and, finally, full circles represent configurations allowed for any value of $\tan\beta$ ($1.01 \leq \tan\beta < 50$). The dark area is the region excluded by current LEP data [14]. We see that, for relatively small values of $\tan\beta$, the region in the μ–M_2 plane which is compatible with set T is quite restricted. The reason for this relies on the fact that for small $\tan\beta$ the neutralino–nucleus interaction is somewhat smaller with respect to higher values of $\tan\beta$, where the coupling to quarks is enhanced, both for the Higgs and squark exchanges. Therefore, lower values of $\tan\beta$ allow the quantity $\xi\sigma_{\rm scalar}^{\rm (nucleon)}$ to be compatible with set T only in the lower edge of the region plotted in Fig.3, where the neutralino mass is constrained to a relatively small range. This property can be seen more clearly in Fig.5, where the gray area denotes, for different values of $\tan\beta$, the neutralino mass ranges compatible with set T. The dark area on the left side of the figure is the region excluded by current LEP data [14]. The region on the left of the vertical solid line around $m_\chi \simeq 50$ GeV is the region explorable by LEP at $\sqrt{s} = 192$ GeV [23]. We notice that, as far as the neutralino sector is concerned, LEP will be able to investigate only marginally the region of parameter space singled out by set T. A better chance to explore the neutralino mass range compatible with set T is given by the future upgrades at the Tevatron and by LHC. As an example, the region which extends up to the vertical dashed line is the mass region which, under favourable hypothesis, will be possibly explored by TeV33 [24].

To complement the information given by the previous figure on the neutralino properties for set T, we show in Fig.6 the neutralino composition for different values of $\tan\beta$. The neutralino composition is parametrized in terms of the fractional amount of gaugino fields in the neutralino mass eigenstate, i.e. $P = a_1^2 + a_2^2$. The two solid lines delimit the region of the neutralino composition explored in our analysis, because of the adopted grid over the supersymmetric parameters. We notice that for small values of $\tan\beta$ the neutralino is constrained around configurations of maximal mixing. This is again related to the necessity, for small values of $\tan\beta$, to have a sufficiently strong coupling to the nucleus, and this happens mainly for maximal mixed states, both in the case of Higgs– and of squark–exchanges. For higher values of $\tan\beta$ and for $P \sim 0.1$, many configurations are excluded by the constraints on Φ_μ.

Let us now discuss the properties of the configurations of set T with respect to the other supersymmetric parameters not discussed before, i.e. m_A, m_0 and A. These parameters, together with $\tan\beta$ and μ, determine the masses of the particles exchanged in the neutralino–nucleus scattering diagrams, which are crucial in establishing the size of both direct and

indirect detection signals. The most interesting characteristic of the configurations of set T is shown in Fig.7, where $\tan\beta$ is plotted against the mass of the lightest neutral Higgs field h. The dark regions are the regions which are excluded by current LEP searches [14] (on the left of the plot) or by theoretical arguments (on the right side). The gray area corresponds to values of m_h and $\tan\beta$ compatible with the properties of set T. For low values of $\tan\beta$ only light Higgs masses are possible ($m_h \lesssim 100$ GeV for $\tan\beta \lesssim 5$), because the small neutralino–nucleus coupling has to be compensated by a light exchanged Higgs particle in order to match the required values of $\xi\sigma_{\rm scalar}^{\rm (nucleon)}$ of set T. For larger values of $\tan\beta$, higher values of m_h are possible. However, the region of light m_h and $\tan\beta \gtrsim 20$ is not compatible with set T because it provides neutrino fluxes from the Earth and the Sun which exceed the bounds of Fig.2. In Fig.7 it is also reported the region which will be accessible to LEP at $\sqrt{s} = 192$ GeV, with a luminosity of 150 pb^{-1} per experiment [23]. A large portion of the region compatible with the modulation analysis will be covered by the LEP analysis. In particular, all the region for $\tan\beta \lesssim 3$ will be analyzed. Thus, the discovery potential of LEP2 for configurations of set T concerns mainly the possible discovery of a light Higgs boson. However, direct confirmation of existence of a chargino and/or a neutralino with the required properties will very likely demand future experiments at Tevatron and LHC.

In the previous discussion we have analyzed the characteristics of the configurations of set T which turn out to be more interesting, especially in connection with the discovery potential at the accelerators in the near future. Furthermore, our analysis has pointed out other features. We only quote here that the configurations of set T do not show correlations with respect to the squark masses in the physical range explored by the present analysis, except in the case of the stop mass, where masses of the lightest stop lighter than 400 GeV are preferred. As regards the stop and sbottom mixing angles, set T is compatible mainly with negative values around the maximally mixed configurations: -0.8 rad $\lesssim \theta_{\tilde{b}} \lesssim -0.3$ rad for the sbottom mixing angle and $\theta_{\tilde{t}} \lesssim -0.8$ rad for the stop. Only a few configurations are compatible with set T in the case of positive mixing angles, again around the maximal squark mixing. This property about the squark mixing angles is reversed for $\mu < 0$: in this case the preferred region is for positive values of the mixing angles, around the value of maximal mixing.

Fig.8 shows the neutralino relic abundance $\Omega_\chi h^2$ as a function of the neutralino mass m_χ for the configurations of set T. The horizontal line denotes the value of $(\Omega h^2)_{\rm min} = 0.03$ which we are adopting here for the rescaling procedure, as discussed in Sect.II B. The most interesting feature of Fig.8 is that many configurations provide a sizeable value for the relic abundance. Some values of the parameters give $\Omega_\chi h^2$ close to 1. It is remarkable that many supersymmetric configurations of set T provide a neutralino with the prerequisites for being a good dark matter candidate [20].

In order to investigate a little further the characteristics of the configurations of set T which provide sizeable neutralino relic abundance, we display in the previously discussed figures the regions where $\Omega_\chi h^2 > 0.1$ (we name as set V the portion of set T which satisfies this requirement). In Fig.5, the region contained inside the long dashed line represent, for each value of $\tan\beta$, the intervals of m_χ compatible with set V. Only values of $\tan\beta \lesssim 20$ are possible, due to the fact that large values of $\tan\beta$ provide large annihilation cross sections, with the consequence of reducing the relic abundance. The neutralino mass intervals compatible with set V appears not to be accessible to LEP at $\sqrt{s} = 192$ GeV [23], but they

could be throughly explored by TeV33 [24].

In Fig.6 the information of the neutralino configurations compatible with set V are reported in the P–$\tan\beta$ plane (regions below the dashed line). For high values of $\tan\beta$, compositions which are purer in the gaugino or higgsino sector are favoured, because they depress the annihilation cross section. On the contrary, for low values of $\tan\beta$, mixed neutralino configurations are compatible with cosmologically relevant values of $\Omega_\chi h^2$. The configurations of set V are also plotted in the $\tan\beta$–m_h plane in Fig.7. Again, the region under discussion is the one inside the dashed line. It is interesting that the cosmologically appealing configurations could be extensively explored by the LEP runs at $\sqrt{s} = 192$ GeV, as far as the Higgs searches are concerned.

Finally, let us remark that the analysis which has been discussed so far in this Section refers to positive values of μ. For $\mu < 0$, our analysis has shown that the situation is, in general, similar to the case of $\mu > 0$, apart from the already quoted properties of the squark mixing angles. However, a few important exceptions are present: i) $\tan\beta$ is constrained to be greater than approximately 3; ii) the neutralino relic abundance does not reach values as high as in the $\mu > 0$ case and it is always less than roughly 0.3.

IV. CONCLUSIONS

In the present paper we have analyzed the properties of neutralinos under the hypothesis that some preliminary experimental results of the DAMA/NaI Collaboration [4] may be indicative of a yearly modulation effect. As stressed by the same Collaboration, this possible indication requires confirmation by the collection and analysis of a much higher statistically significant set of data, now under way. Motivated by the intriguing possibility that the effect is real and due to a supersymmetric relic particle (neutralino), we have examined which supersymmetric configurations would be singled out by the DAMA/NaI data. We have shown that some of these configurations are excluded by current bounds due to up–going muon fluxes from the Sun and the Earth. However, most remarkably a large sample of supersymmetric configurations relevant for the possible modulation effect are compatible with all available experimental data, in ranges of the supersymmetric parameters largely accessible to future investigation at accelerators. Also, indirect search for relic neutralinos with neutrino telescopes of larger exposure will be capable of providing most valuable information on this matter. The discovery potential of other experimental means, in particular $\bar{p}/p$ ratio in cosmic rays [25,26], will be analyzed elsewhere [27]. An important result of the present study is that a number of the analyzed supersymmetric configurations would entail a neutralino with a sizeable contribution to the cosmological matter density.

A further word of caution has to be added here. The analysis presented in the present paper relies on the use of a specific set for the values of the astrophysical parameters (set I of Table 1). This set corresponds to the median values for these parameters. Should the astrophysical parameters be on the unfavorable side (set II of Table 1), only a very limited sample of supersymmetric configurations would be compatible with the region R_m singled out by the data of Ref. [4].

Acknowledgements. We thank the DAMA/NaI Collaboration for making their data available to us before publication. We also express our thanks to R. Bernabei, P. Belli, A. Incicchitti and D. Prosperi for very fruitful discussions about the significance of the experimental results examined in the present paper.

TABLES

TABLE I. Values of the astrophysical and cosmological parameters relevant to direct and indirect detection rates. $V_{\rm r.m.s.}$ denotes the root mean square velocity of the neutralino Maxwellian velocity distribution in the halo, $V_{\rm esc}$ is the neutralino escape velocity and $V_\odot$ is the velocity of the Sun around the galactic centre; $\rho_{\rm l}$ denotes the local dark matter density and $(\Omega h^2)_{\rm min}$ the minimal value of Ωh^2. The values of set I are the median values of the various parameters, the values of set II are the extreme values of the parameters which, within the physical ranges, provide the lowest estimates of the detection rates (once the supersymmetric parameters are fixed).

	Set I	Set II
$V_{\rm r.m.s}({\rm km\cdot s^{-1}})$	270	245
$V_{\rm esc}({\rm km\cdot s^{-1}})$	650	450
$V_\odot({\rm km\cdot s^{-1}})$	232	212
$\rho_{\rm l}({\rm GeV\cdot cm^{-3}})$	0.5	0.2
$(\Omega h^2)_{\rm min}$	0.03	0.3

Figure Captions

Figure 1 – The scalar neutralino–nucleon cross section $\sigma_{\rm scalar}^{\rm (nucleon)}$, multiplied by the scaling factor ξ, is plotted versus the neutralino mass m_χ. The closed contour delimits the region (defined as R_m in the text) singled out at 90% C.L. when the data of ref. [4] are interpreted in terms of a modulation signal. The open curve denotes the 90% C.L. upper bound obtained from the total counting rates of Ref. [2]. The scatter plot represents the theoretical prediction for $\xi\sigma_{\rm scalar}^{\rm (nucleon)}$, calculated within the MSSM scheme. Only configurations with $\mu > 0$ are displayed. The neutralino configurations which fall inside R_m are defined as set S. The cosmological and astrophysical parameters of set I of Table 1 are used.

Figure 2a – Flux of up-going muons $\Phi_\mu^{\rm Earth}$ as a function of m_χ, calculated for the neutralino configurations belonging to set S. The solid line represents the experimental 90% C.L. upper bound of Ref. [21]. Cosmological and astrophysical parameters are the same as those in Fig.1.

Figure 2b – Flux of up-going muons $\Phi_\mu^{\rm Sun}$ as a function of m_χ, calculated for the neutralino configurations belonging to set S. The solid line represents the experimental 90% C.L. upper bound of Ref. [21]. Cosmological and astrophysical parameters are the same as in Fig.1.

Figure 3 – Neutralino configurations of set S that survive indirect search bounds (referred to as set T in the text). All configurations falling out of region R_m have been dropped.

Figure 4 – Neutralino configurations of set T displayed in the μ–M_2 plane. The dark area is excluded by accelerator constraints. Dots denote configurations with $10 \leq \tan\beta < 50$; stars denote configurations with $5 \leq \tan\beta < 50$; full circles represent configurations allowed for any value of $\tan\beta$ ($1.01 \leq \tan\beta < 50$).

Figure 5 – The configurations compatible with set T are plotted in the m_χ–$\tan\beta$ plane, within the gray area. The dark region on the left side is excluded by current LEP data [14]. The region on the left of the vertical solid line will be accessible to LEP at $\sqrt{s} = 192$ GeV [23]. The region on the left of the vertical dashed line will be explorable at TeV33 [24]. In the region delimited by the closed dashed line the neutralino relic abundance $\Omega_\chi h^2$ may exceed 0.1.

Figure 6 – The configurations compatible with set T are plotted in the P–$\tan\beta$ plane (dots). On the left part of the horizontal axis the gaugino fractional amount P is given, whereas on the right part of the same axis the complementary variable $1 - P$ is reported. The two solid lines delimit the region of the neutralino composition explored in our analysis. Configurations which provide $\Omega_\chi h^2 > 0.1$ fall below the dashed line.

Figure 7 – The configurations compatible with set T are plotted in the m_h–$\tan\beta$ plane, within the gray area. The dark regions are excluded by current LEP searches [14] or by theoretical arguments. Configurations which provide $\Omega_\chi h^2 > 0.1$ fall within the region delimited by the closed dashed line. The region on the left of the solid line will be accessible to LEP at $\sqrt{s} = 192$ GeV, with a luminosity of 150 pb^{-1} per experiment [23].

Figure 8 – Neutralino relic abundance $\Omega_\chi h^2$ as a function of the neutralino mass m_χ, calculated for the neutralino configurations of set T. The horizontal line denotes the value of $(\Omega h^2)_{\rm min}$=0.03.

REFERENCES

[1] A. Bottino, F. Donato, G. Mignola, S. Scopel, P. Belli and A. Incicchitti, Phys. Lett. B 402 (1997) 113.

[2] R. Bernabei et al., Phys. Lett. B 389 (1996) 757.

[3] See, for instance, Proc. Int. Workshop on Identification of Dark Matter, Sheffield, September 1996.

[4] R. Bernabei et al., ROM2F/97/33; P. Belli, talk at TAUP97, Laboratori Nazionali del Gran Sasso, September 7, 1997.

[5] H.P. Nilles, Phys. Rep. 110 (1984) 1; H.E. Haber and G.L. Kane, Phys. Rep. 117 (1985) 75; R. Barbieri, Riv. Nuovo Cim. 11 (1988) 1.

[6] For a thorough list of references previous to 1996, see G. Jungman, M. Kamionkowski and K. Griest, Phys. Rep. 267 (1996) 195.

[7] A. Bottino, N. Fornengo, G. Mignola and L. Moscoso, Astropart. Phys. 3 (1995) 65.

[8] L. Bergström, J. Edsjö and M.Kamionkowski, Astropart. Phys. 7 (1997) 147.

[9] A. Bottino, V. de Alfaro, N. Fornengo, G. Mignola and M. Pignone, Astropart. Phys. 2 (1994) 67.

[10] J. Edsjö and P. Gondolo, Phys. Rev. D 56 (1997) 1879.

[11] A. Bottino, V. de Alfaro, N. Fornengo, G. Mignola and S. Scopel, Astropart. Phys. 2 (1994) 77.

[12] L.Bergström and P. Gondolo, Astropart. Phys. 5 (1996) 263.

[13] A. Bottino, Proc. Int. Workshop on Identification of Dark Matter, Sheffield, September 1996, astro-ph/9611137.

[14] ALEPH Collab., CERN–PPE/97–041, April 1997; ALEPH Collab., CERN–PPE/97–056, May 1997; ALEPH Collab., CERN–PPE/97–071, June 1997; A. De Min, DELPHI Collab., Talk at the 3rd Warsaw Workshop 'Physics from the Planck scale to the electroweak scale', Warsaw, April 1997; DELPHI Collab., CERN–PPE/97–085, July 1997; F. Di Lodovico, L3 Collab., Talk at the 3rd Warsaw Workshop 'Physics from the Planck scale to the electroweak scale', Warsaw, April 1997; OPAL Collab., CERN–PPE/97–046, April 1997; OPAL Collab., CERN–PPE/97–083, July 1997.

[15] M.S. Alam et al. (CLEO Coll.), Phys. Rev. Lett. 74 (1995) 2885.

[16] R. Barbieri, M. Frigeni and G.F. Giudice, Nucl. Phys. B 313 (1989) 725.

[17] K. Griest, Phys. Rev. D 38 (1988) 2357; Phys. Rev. Lett. 61 (1988) 666.

[18] S. Scopel, Proc. Int. Workshop on Aspects of Dark Matter in Astro- and Particle Physics, Heidelberg, September 1996.

[19] K. Griest and D. Seckel, Phys. Rev. D 43 (1991) 3191; S. Mizuta and M. Yamaguchi, Phys. Lett. B 298 (1993) 120.

[20] V. Berezinsky, A. Bottino, J. Ellis, N. Fornengo, G. Mignola and S.Scopel, Astropart. Phys. 5 (1996) 333.

[21] Baksan Collab., Proc. 4th Int. Neutrino Conference, Heidelberg, April 1997

[22] F. Ronga, Macro Collab. Proc. 25th Int. Cosmic Ray Conference (ICRC 97), Durban, South Africa, July 1997.

[23] Physics at LEP2, editors G. Altarelli, T. Sjöstrand and F. Zwirner, CERN 96–01, February 1996.

[24] Report of the TeV–2000 Study Group, editors D. Amidei and R. Brock, FERMILAB–PUB–96/082, April 1996.
[25] A. Bottino, C. Favero, N. Fornengo and G. Mignola, Astropart. Phys. 3 (1995) 77.
[26] G. Mignola, Proc. Int. Workshop on Identification of Dark Matter, Sheffield, September 1996, astro-ph/9611138.
[27] A. Bottino, F. Donato, N. Fornengo and S. Scopel, in progress.

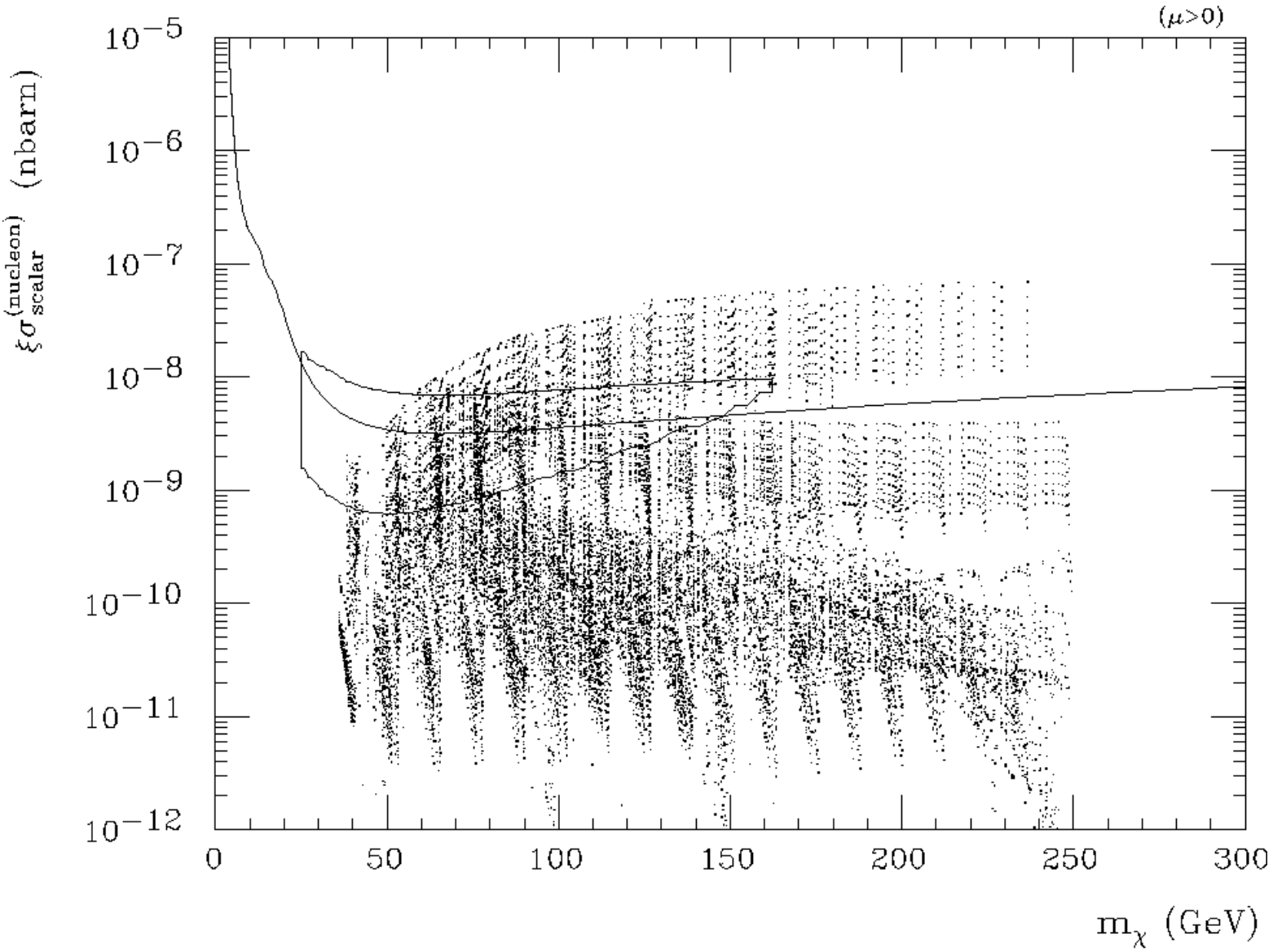
(μ>0)
10^{-5}
10^{-6}
10^{-7}
10^{-8}
10^{-9}
10^{-10}
10^{-11}
10^{-12}
$\xi\sigma_{scalar}^{(nucleon)}$ (nbarn)
0
50
100
150
200
250
300
m_χ (GeV)

Figure 1

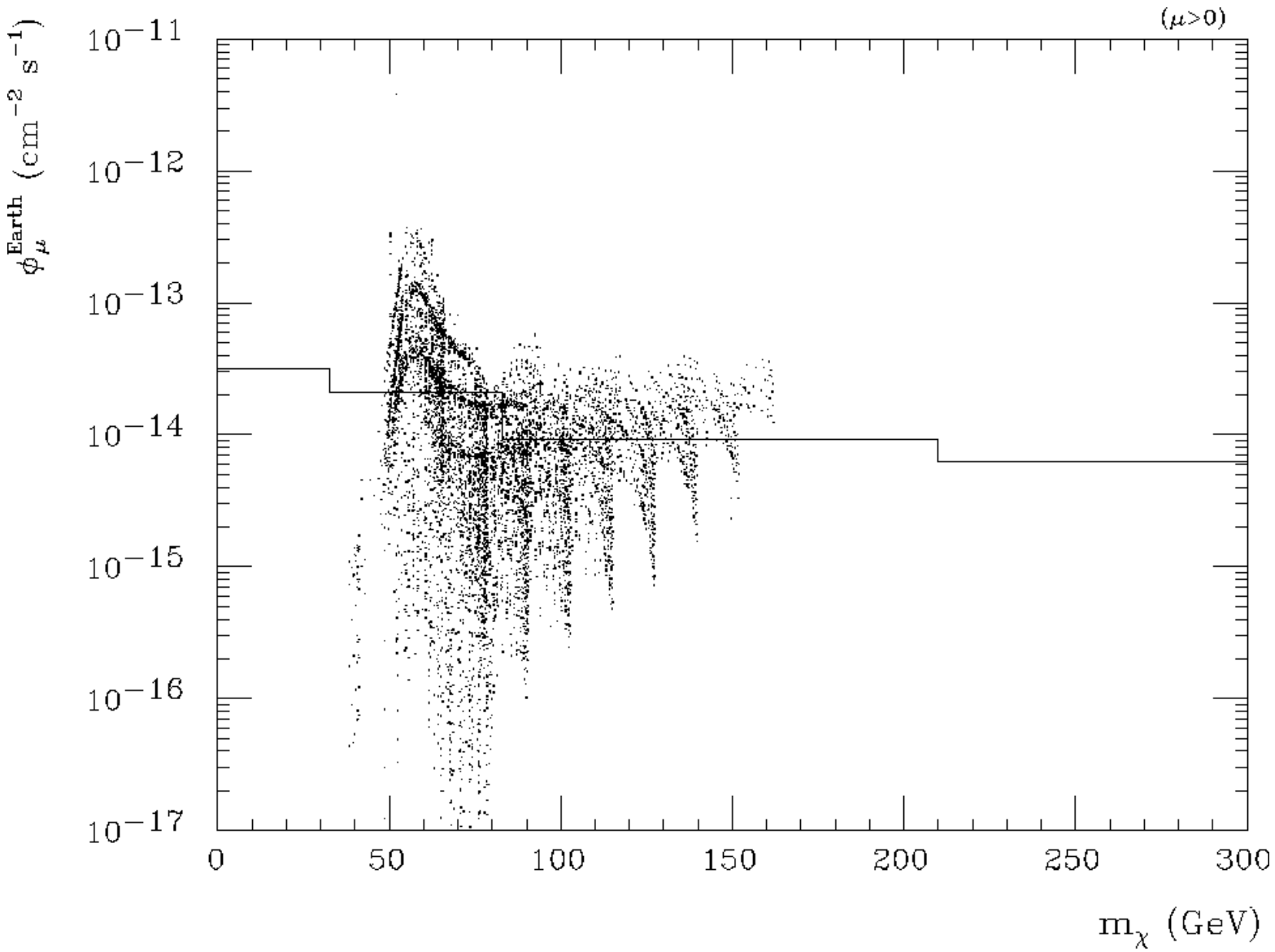
$(\mu>0)$
$\phi_\mu^{\rm Earth}$ (cm^{-2} s^{-1})
10^{-11}
10^{-12}
10^{-13}
10^{-14}
10^{-15}
10^{-16}
10^{-17}
0
50
100
150
200
250
300
m_χ (GeV)

Figure 2a

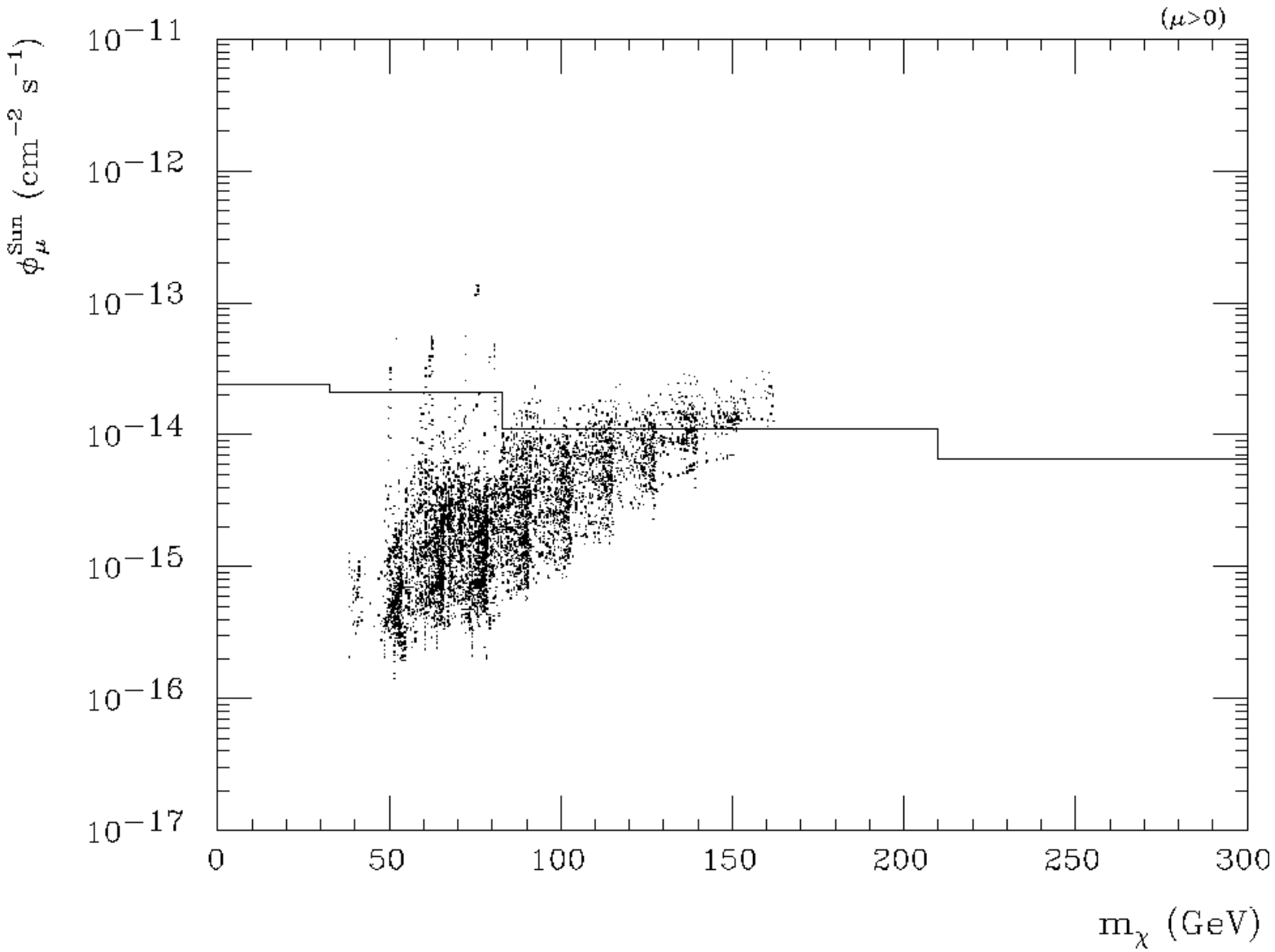
$(\mu>0)$
$\phi_\mu^{\rm Sun}$ (cm^{-2} s^{-1})
10^{-11}
10^{-12}
10^{-13}
10^{-14}
10^{-15}
10^{-16}
10^{-17}
0
50
100
150
200
250
300
m_χ (GeV)

Figure 2b

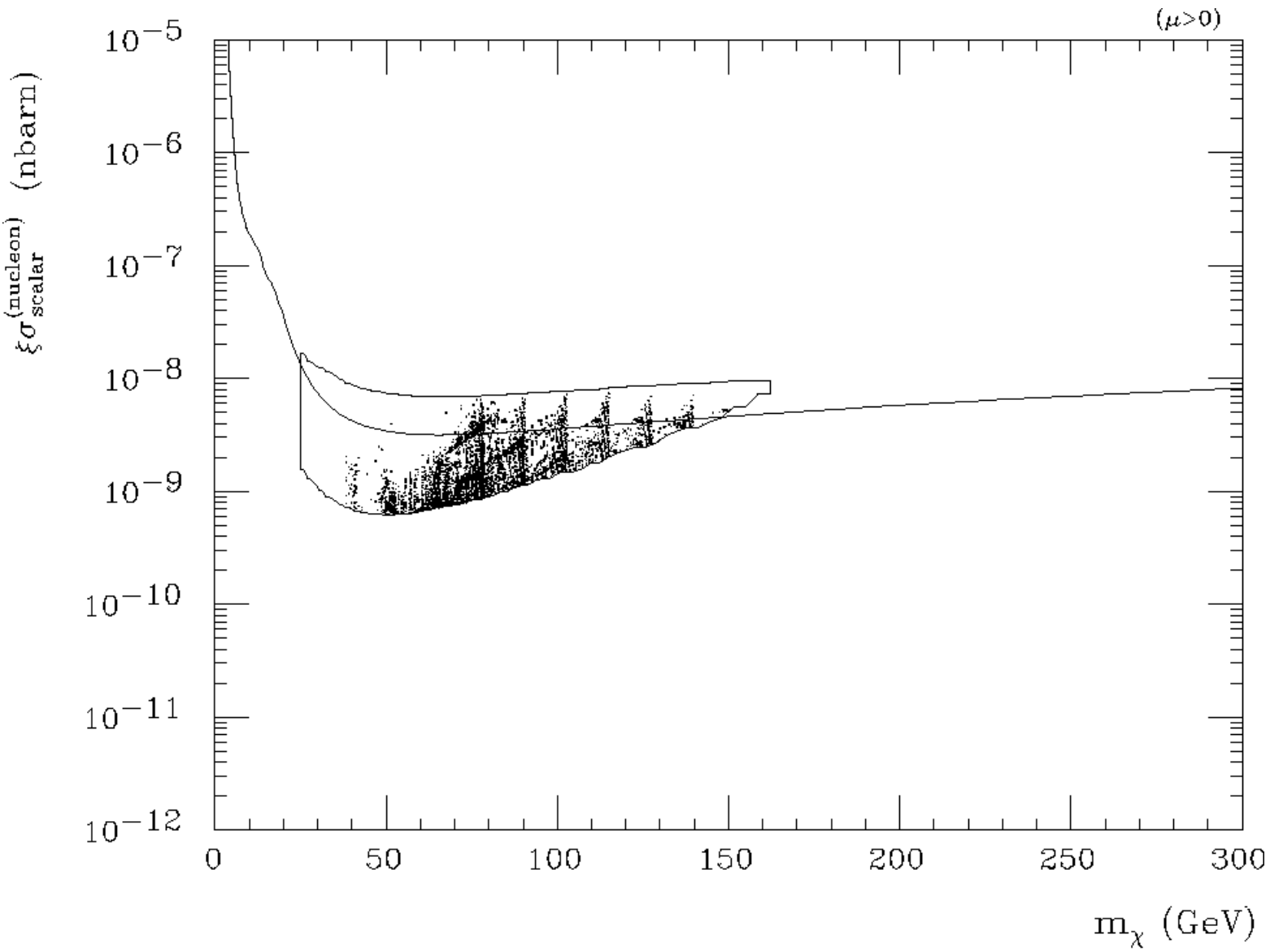
(μ>0)
10^{-5}
10^{-6}
10^{-7}
10^{-8}
10^{-9}
10^{-10}
10^{-11}
10^{-12}
$\xi\sigma_{scalar}^{(nucleon)}$ (nbarn)
0
50
100
150
200
250
300
m_χ (GeV)

Figure 3

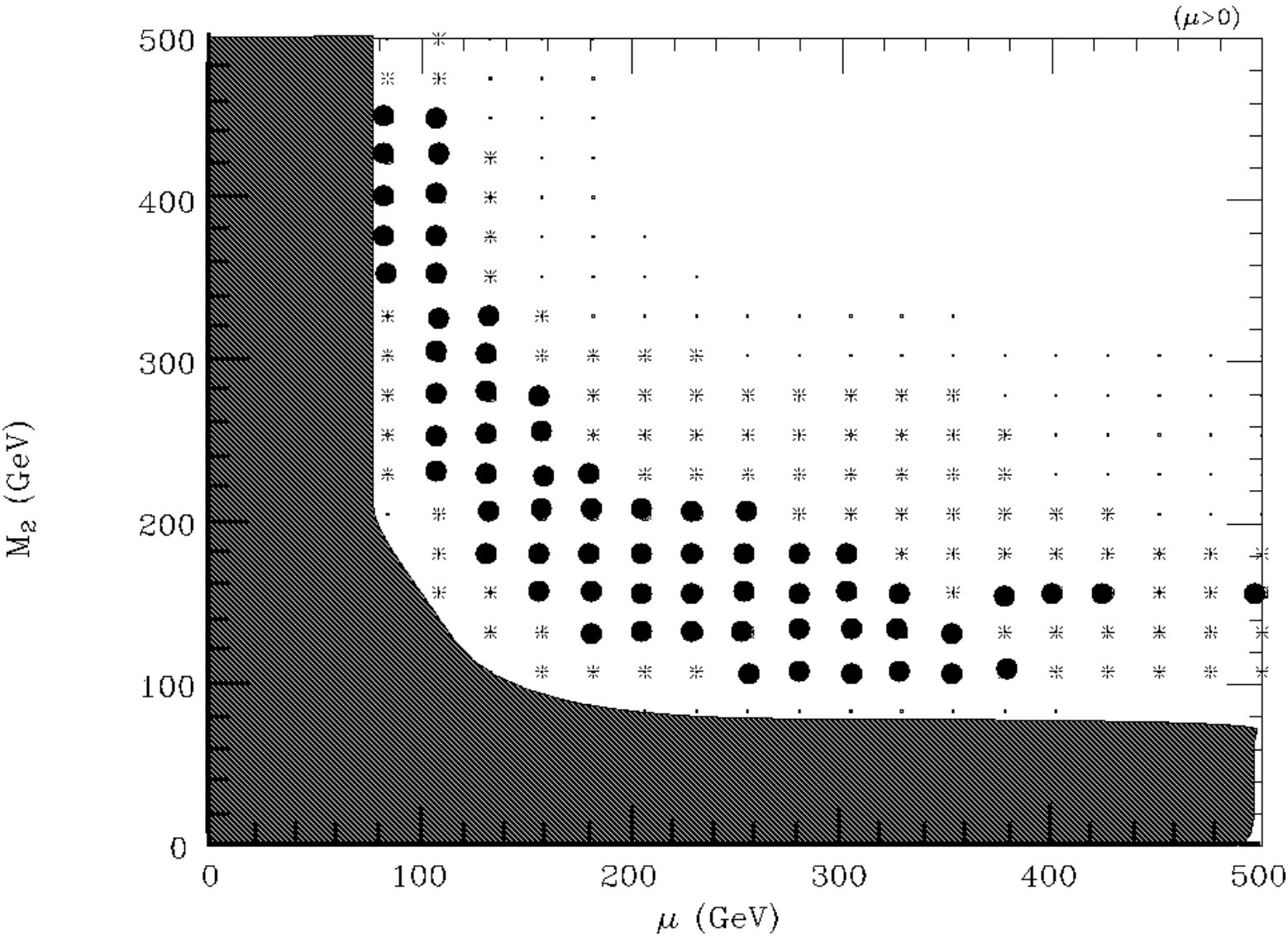

Figure 4

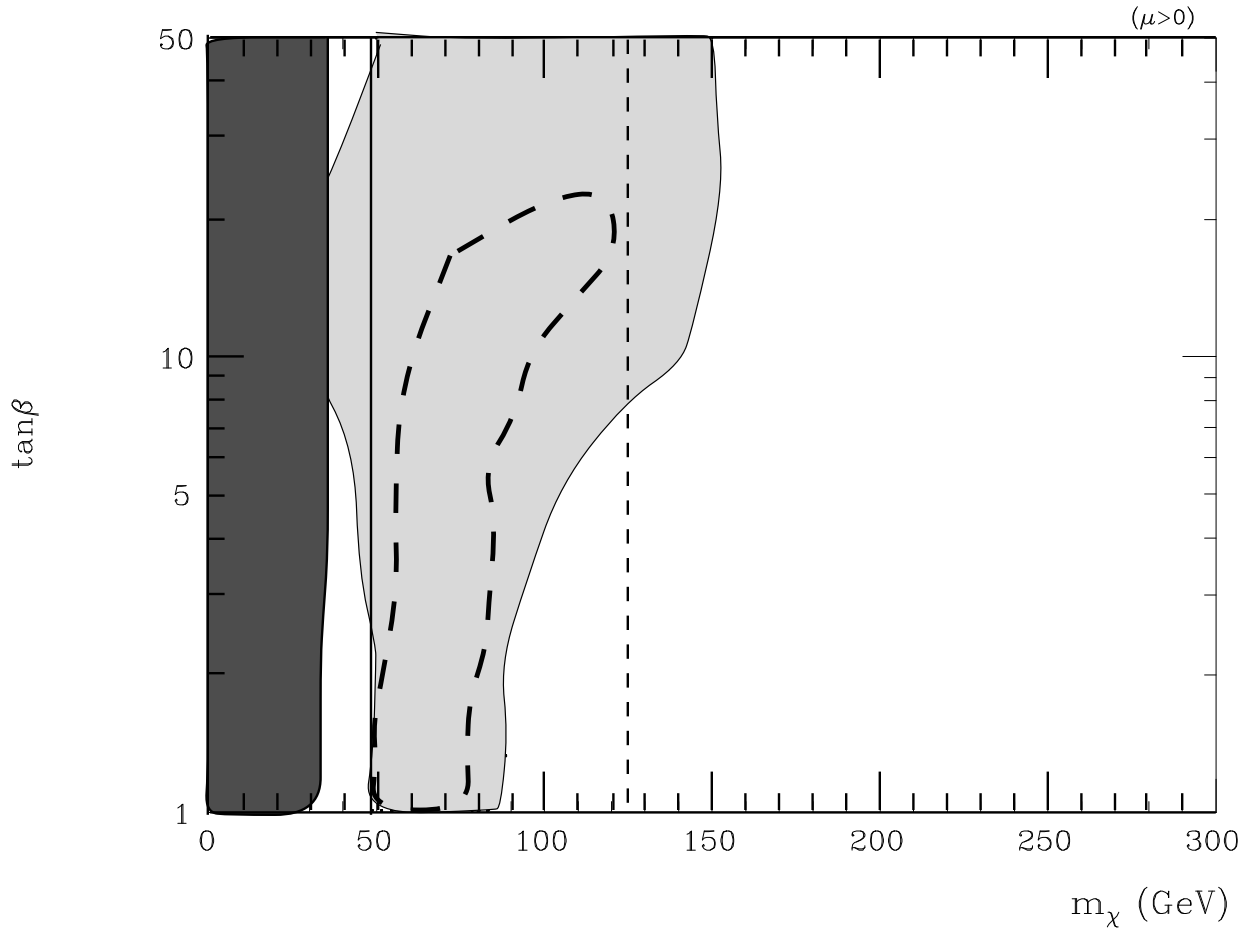

Figure 5

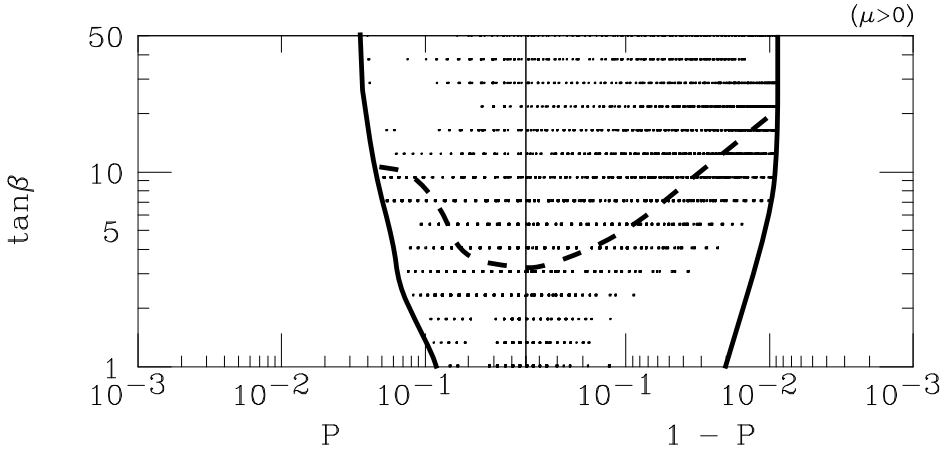

Figure 6

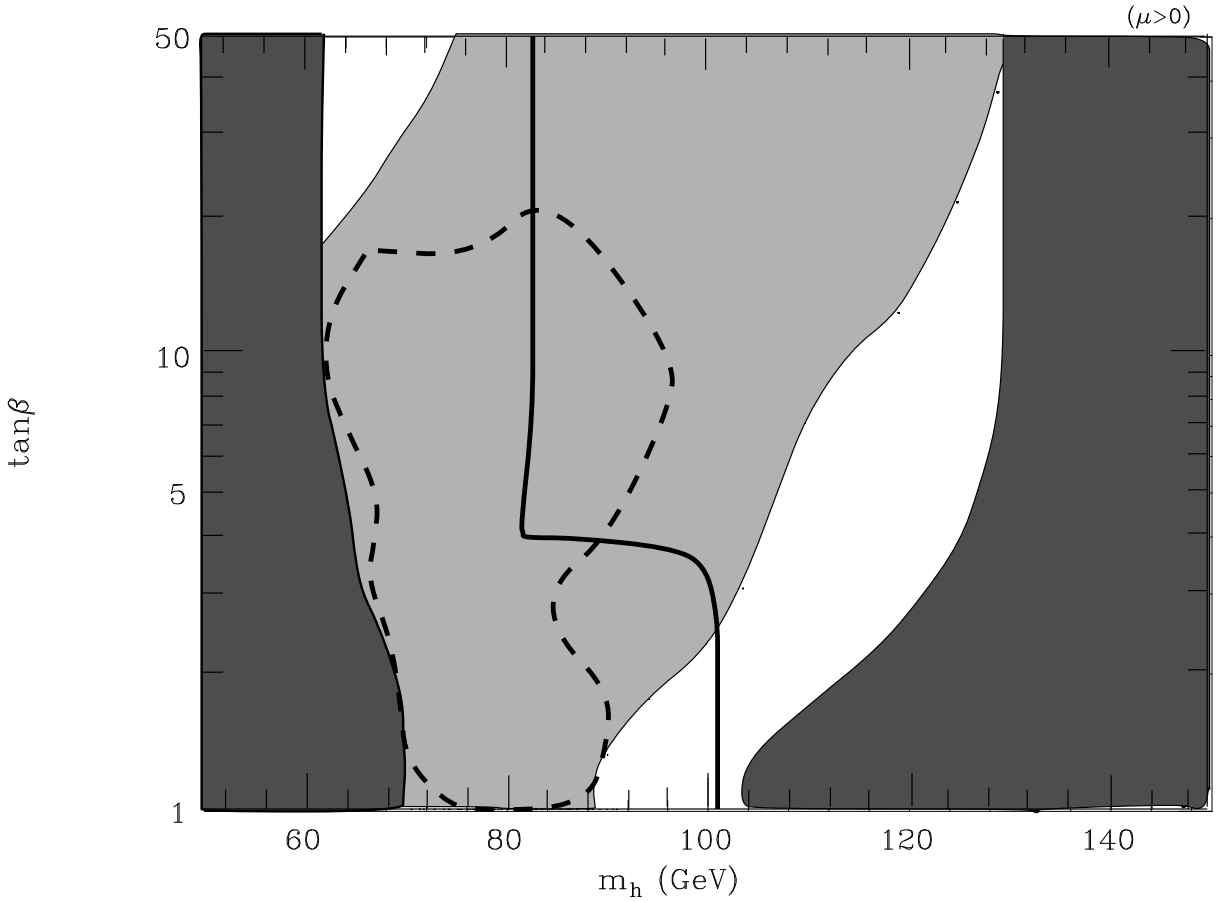

Figure 7

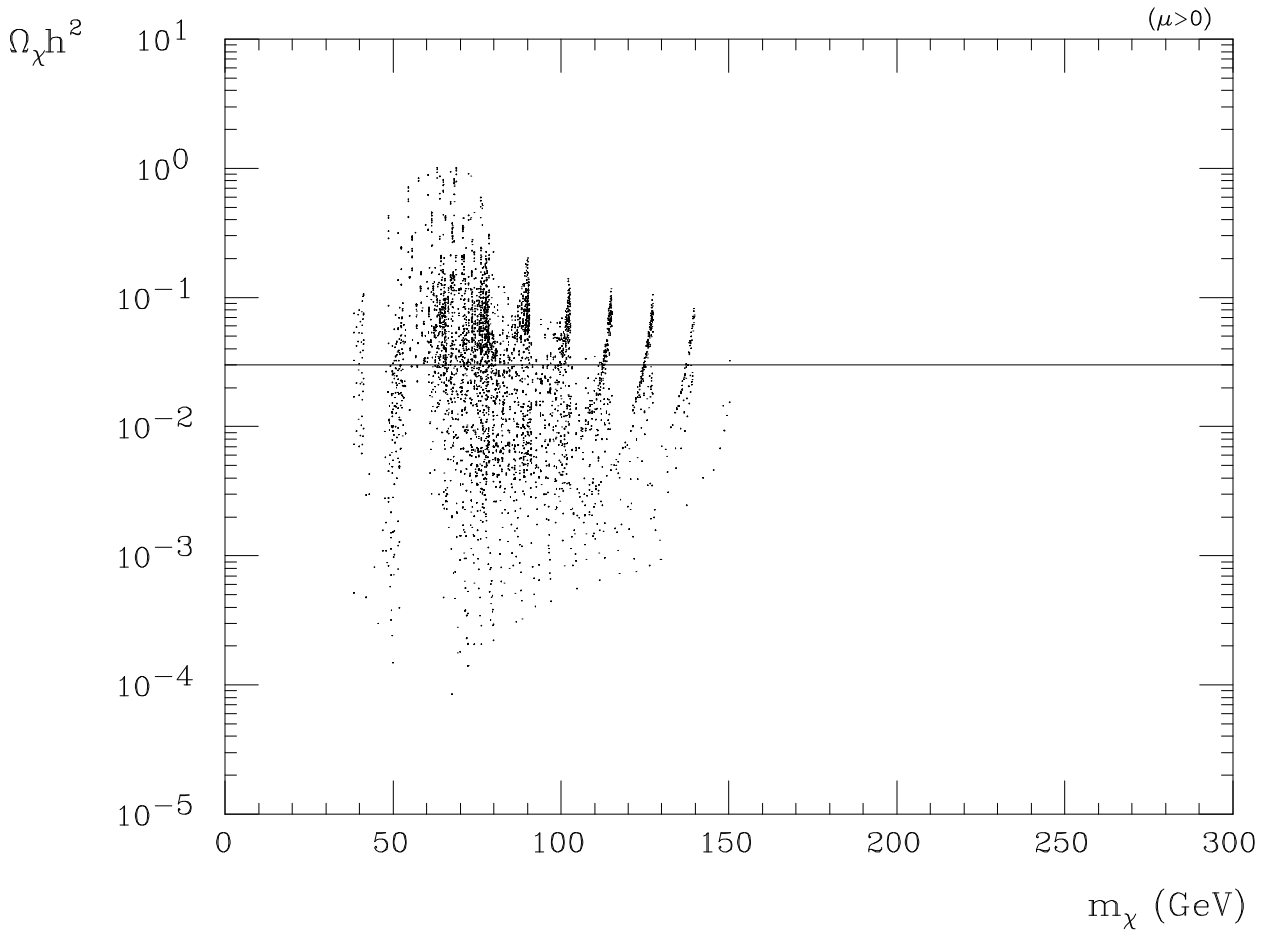
$\Omega_\chi h^2$
$(\mu>0)$
10^1
10^0
10^{-1}
10^{-2}
10^{-3}
10^{-4}
10^{-5}
0
50
100
150
200
250
300
m_χ (GeV)

Figure 8